Probing triple-Higgs productions via 4b2γ decay channel at a 100 TeV hadron collider

Chien-Yi Chen, Qi-Shu Yan, Xiaoran Zhao, Zhijie Zhao, and Yi-Ming Zhong

Phys. Rev. D **93**, 013007 — Published 11 January 2016

DOI: 10.1103/PhysRevD.93.013007

Probing triple-Higgs productions via $4b2\gamma$ at a 100 TeV hadron collider

Chien-Yi Chen[1,2,3], Qi-Shu Yan[4,5,6], Xiaoran Zhao[4], Zhijie Zhao[4,a], Yi-Ming Zhong[7]

[1] Department of Physics, Brookhaven National Laboratory, Upton, New York 11973, USA

[2] Department of Physics and Astronomy, University of Victoria, Victoria, BC V8P 5C2, Canada

[3] Perimeter Institute for Theoretical Physics, Waterloo, ON N2J 2W9, Canada

[4] School of Physical Sciences, University of Chinese Academy of Sciences, Beijing 100049, P. R. China

[5] Center for High-Energy Physics, Peking University, Beijing, 100871, P. R. China

[6] Center for future high energy physics, CAS, P. R. China

[7] C.N. Yang Institute for Theoretical Physics, Stony Brook University, Stony Brook, New York 11794, USA

Abstract

The quartic self-coupling of the Standard Model Higgs boson can only be measured by observing the triple-Higgs production process, but it is challenging for the LHC Run 2 or ILC at a few TeV because of its extremely small production rate. In this paper, we present a detailed MC simulation study of the triple-Higgs production through gluon fusion at a 100 TeV hadron collider and explore the feasibility of observing this production mode. We focus on the decay channel $HHH \to b\bar{b}b\bar{b}\gamma\gamma$, investigating detector effects and optimizing the kinematic cuts to discriminate the signal from the backgrounds. Our study shows that in order to observe the Standard Model triple-Higgs signal, the integrated luminosity of a 100 TeV hadron collider should be greater than 1.8×10^4 ab^{-1}. We also explore the dependence of the cross section upon the trilinear (λ_3) and quartic (λ_4) self-couplings of the Higgs. We find that, through a search in the triple Higgs production, the parameters λ_3 and λ_4 can be restricted to the ranges $[-1, 5]$ and $[-20, 30]$, respectively. We also examine how new physics can change the production rate of triple-Higgs events. For example, in the singlet extension of the Standard Model, we find that the triple-Higgs production rate can be increased by a factor of $\mathcal{O}(10)$.

[a] Correspondence Author: zhaozhijie12@mails.ucas.ac.cn

I. INTRODUCTION

The discovery of the Higgs boson with a mass of around 125–126 GeV[1] at the Large Hadron Collider (LHC) [1, 2] makes it possible to understand electroweak symmetry breaking (EWSB) in detail. To obtain the full knowledge of EWSB, an important task is to measure the Higgs couplings so as to determine whether its properties agree with the Standard Model (SM) predictions. In particular, the measurement of Higgs self-couplings is crucial because it is the only way to reconstruct and verify the scalar potential [3], which can be directly related to our understanding of baryogenesis [4] and vacuum stability. In the second part of this paper, we use the singlet extension of the SM to demonstrate how the scalar potential can be affected by new physics.

In the language of an effective field theory, we can parameterize the Higgs self-interaction Lagrangian as:

$$L \supset -\frac{1}{2}m_H^2 H^2 - \lambda_3 \lambda_{SM} v H^3 - \frac{1}{4}\lambda_4 \lambda_{SM} H^4 + \cdots , \tag{1}$$

where higher dimensional operators denoted by an ellipsis, like operators $H\partial H \cdot \partial H$ studied in [5] and H^5, are neglected here. In Eq. (1), $v = 246$ GeV is the Higgs field vacuum expectation value (vev) and $m_H = 126$ GeV is the Higgs boson mass. In this Lagrangian, we define two free parameters, λ_3 and λ_4, to describe the triple- and quartic-Higgs vertices, respectively:

$$g_{HHH} = 6\lambda_3 \lambda_{SM} v, \;\; g_{HHHH} = 6\lambda_4 \lambda_{SM}. \tag{2}$$

In the SM, these two free parameters are equal to one, i.e. $\lambda_3 = \lambda_4 = 1$ and all higher dimensional operators vanish. The self-coupling parameter λ_{SM} is related to m_H by $\lambda_{SM} = m_H^2/2v^2$. Due to the fact that $\lambda_{SM} \approx 0.13$, the range of λ_4 can be taken to be around 20 (its sign is undetermined) in order to guarantee either the validity of perturbation method or the unitary bound.

Recently, the di-Higgs production at LHC [8–11, 22] has been a hot topic due to its sensitivity to g_{HHH} and λ_3. It is well-known that gluon fusion is the dominant process for di-Higgs production at the LHC, and decay channels like $b\bar{b}\gamma\gamma$ [12, 13], $b\bar{b}\tau\tau$ [14, 15], $b\bar{b}WW$ [16] and $b\bar{b}b\bar{b}$ [17] have been well studied. Previous studies show that the triple self-coupling

[1] We use $m_H = 126$ GeV in this study. Recent results from the LHC collaborations suggest $m_H = 125$ GeV. This change in m_H barely affect our results.

can be measured within 40% accuracy at LHC Run 2 [10, 18]. The double Higgs production at a 100 TeV hadron collider has also been studied [19, 20]. A study on $HH \to WW^*WW^*$ shows that the sensitivity can reach up to 13σ in the SM [21].

In contrast, very little attention has been paid to triple-Higgs production. Early work on triple-Higgs production has shown that in the SM it is very challenging to discover the signals at e^+e^- colliders, because the cross section of $e^+e^- \to ZHHH$ is very small. For example, the cross section is only 0.4 ab at $\sqrt{s} = 1$ TeV [23] and the total production is just 1.2 events for a designed integral luminosity 3 ab^{-1}. However, the triple-Higgs production rate can be enhanced dramatically if there is an extended Higgs sector. The cross section of triple-Higgs production can be at $\mathcal{O}(0.1)$ pb in the Two-Higgs-Doublet Model (2HDM) [24, 25]. So the triple-Higgs production at e^+e^- colliders is an important process to probe new physics. It is also remarkable that the Higgs self-couplings could be measured to some degree via indirect or loop processes at e^+e^- colliders [26].

The cross section of triple-Higgs production at hadron colliders was calculated in [27, 28]. Its SM value, via gluon fusion, is $\mathcal{O}(0.01)$ fb at 14 TeV LHC, which is too small to be observed with the current designed luminosity. Moreover, the dominant contribution of this process is the top-loop pentagon diagram [28], which suggests that measurement of λ_4 is very challenging even if the triple-Higgs production is discovered. (λ_4 can be read out from the fit cross section given in Eq. (6).) In this case, the top mass effect is crucial and leads to a K-factor which is similar to the di-Higgs case. A more precise prediction of triple-Higgs production at 100 TeV can be found in the Ref. [29], where it is shown that the cross section can be increased from 3 fb to 5 fb after taking into account the next-to-leading-order (NLO) corrections.

If we can suppress the SM backgrounds effectively or increase the integrated luminosity enough, it is still possible to observe this process at a 100 TeV machine. Recently, the channel $pp \to HHH \to b\bar{b}b\bar{b}\gamma\gamma$ at hadron level (with part of detector simulations implemented) is studied in [30]. We will comment on it in Section VI.

Although the cross sections of triple-Higgs production have been studied, to our knowledge, serious feasibility studies are still absent in the literature. In this paper, we will focus on the feasibility of triple-Higgs production at a future 100 TeV hadron collider via $b\bar{b}b\bar{b}\gamma\gamma$ so as to fill this gap. We includes detector simulations by using DELPHES 3.0 [31, 32]. We explore the following three questions related to the physics of a 100 TeV collider.

1. What is the minimal luminosity to observe the signature of triple Higgs production via $4b2\gamma$[2] final state in the standard model at a 100 TeV collider after taking into account more realistic detector effects?

2. What are the bounds on the trilinear and quartic couplings λ_3 and λ_4 defined in Eq. (1) that we can achieve by using the triple Higgs production signature?

3. What is the potential to discover new physics via the observation of the final states of triple Higgs bosons? We will use the singlet+SM model as an example to demonstrate this potential.

The structure of this paper is organized as follows. In Section II, we describe our Monte Carlo (MC) simulation method. Our analysis is mainly demonstrated in Section III. The SM results are presented as a standard candle and the kinematic cuts are explored and exposed. We also apply two multivariate analysis methods to improve the signal and background discrimination. Based on those analysis methods, we can determine the integrated luminosity for discovering the triple-Higgs boson final states. In Section IV, the sensitivity of Higgs quartic couplings in the effective Lagrangian are addressed. In Section V, the triple-Higgs production in the singlet+SM model is presented. We end this work with some discussions and future outlook.

II. THE MC SIMULATION

We use MadLoop/aMC@NLO [33] and GoSam [34] to generate the matrix elements of triple-Higgs production via gluon fusion. Then we use the VBFNLO code [35–37] to perform the phase space integration, where we set the parton distribution functions (PDFs) as CTEQ6L1 [38].

As a cross check, our code yields a cross section $\sigma_{14\ \mathrm{TeV}} = 6.67 \times 10^{-2}$ fb for the same parameters given by [28]. The two results agree. To arrive at this result we choose the phase space cuts for the final Higgs bosons as $|\eta(H)| < 5.0$ and $P_t(H) > 1$ GeV. Then we set both the renormalization scale and the factorization scale to be the invariant mass of the final states. Our code also performs a reweighting in order to generate unweighted parton level

[2] We use the shorthand, for example, '$2b$' or '$4b$' to denote $b\bar{b}$ or $b\bar{b}b\bar{b}$, respectively.

events. After finishing these cross checks, we use our code to generate unweighted parton level signal events at the center-of-mass energy of 100 TeV. Higgs bosons decays to $b\bar{b}b\bar{b}\gamma\gamma$ via the DECAY package provided by MadGraph 5. Then we pass each event to PYTHIA 6.4 [39] to simulate the parton shower and to perform hadronization and further decays.

The parton-level background events are generated by MadGraph5/aMC@NLO [40] directly and showered through PYTHIA 8 [41]. In this paper, we only consider events with at least two tagged b-jets, i.e. the $n_b \geq 2$ case (cases with a different number of tagged b-jets are discussed in Section VI). Then we take into account two types of dominant background events: $pp \to b\bar{b}jj\gamma\gamma$ and $pp \to Ht\bar{t}$. To generate the most relevant events, several generator level cuts are applied for $pp \to b\bar{b}jj\gamma\gamma$ event generation: for b-jets, $P_t(b) > 30$ GeV and $|\eta(b)| < 5.0$; for other jets, $P_t(j) > 20$ GeV, $|\eta(j)| < 5.0$; and for γ's,$P_t(\gamma) > 30$ GeV, $|\eta(\gamma)| < 2.5$ and $|M_{\gamma\gamma} - 126 \text{ GeV}| < 15$ GeV, where $M_{\gamma\gamma}$ is the invariant mass of two photons. After those cuts, the cross section of $pp \to b\bar{b}jj\gamma\gamma$, σ_{b1}, is 192.8 fb. We do not introduce any extra generator level cuts for the Higgs or tops in the event generation of $pp \to Ht\bar{t}$. We also require a resonant decay from Higgs to $\gamma\gamma$ when the events are passed to PYTHIA 8. The cross section of $pp \to H(\gamma\gamma)t\bar{t}$, σ_{b2}, with a branching ratio $BR(H \to \gamma\gamma) \approx 0.25\%$, is found to be 68.2 fb.

In order to reduce the fluctuation effects from the MC simulation, we generate 50k, 150k, and 150k events for the signal, $pp \to b\bar{b}jj\gamma\gamma$ background, and $H(\gamma\gamma)t\bar{t}$ background, respectively.

We use FASTJET [42] for jet clustering. Jets are clustered by using the anti-k_t algorithm [43] with a cone of radius $R = 0.5$ and minimum $P_t(j) = 30$ GeV. For photon identification, the maximum of isolation efficiency is 95%, with transverse momentum $P_t(\gamma) > 10$ GeV and $|\eta(\gamma)| \leq 2.5$. The efficiency decreases to 85% for $2.5 < |\eta(\gamma)| \leq 5.0$. Pile-up effects are neglected in this work. The detector simulation is performed by DELPHES 3.0 [31, 32]. Details about the set-up are shown in Appendix A.

The b-tagging is simulated by assuming 60% b-jet efficiency working point. The (mis-)tagging efficiencies vary with respect to different P_t and η of jets. The efficiency curves are given in Appendix B. For $P_t(j) = 120$ GeV, the b-tagging efficiencies for (b, c, light) jets are (0.6, 0.1, 0.001). Those efficiencies dramatically drop down to (0.28, 0.046, 0.001) at $P_t(j) = 30$ GeV.

We neglect the background events from the processes $pp \to HW^+W^-$, because $W^\pm$ is unable to decay to b quarks, and these background events can be efficiently rejected by two b-taggings and its production cross section is much smaller than the process $pp \to t\bar{t}H$. We also neglect the process $pp \to HZZ$. It has a cross section $\sigma_{HZZ} = 29.3$ fb, but its branching ratio of $HZZ \to \gamma\gamma b\bar{b}b\bar{b}$ is smaller than 0.006%. The other backgrounds like $Hb\bar{b}b\bar{b}$ and $b\bar{b}b\bar{b}\gamma\gamma$ can be safely neglected for their small cross sections when compared with the process $pp \to b\bar{b}jj\gamma\gamma$. We also neglect the background process $pp \to HHjj$, because the cross section is much smaller than those of two dominant background processes we considered here.

III. THE ANALYSIS OF THE SM

A. Parton Level Distributions

The leading order cross section of $gg \to HHH$ in the SM is $\sigma_s = 3.05$ fb at a 100 TeV colllider. The invariant mass of a pair of Higgs boson m_{HH} in each event and the invariant mass of final states m_{HHH} distributions are shown in Fig. (1). The NLO corrections for this process is large. Therefore, throughout this paper we assume that the K-factor is 2.0 [30]. The peaks of m_{HH} and m_{HHH} are around 350 GeV and 600 GeV, respectively. The dominant contributions are from box and pentagon diagrams as we will explain in the next section from our fit by Eq. (5). It is noticed that there are long tails in these distributions due to the high centre-of-mass energy.

B. Detector level analysis

Below we focus our analysis on channel $gg \to HHH \to b\bar{b}b\bar{b}\gamma\gamma$, which possesses a branching ratio $\approx 0.15\%$ in the all decay final states. In order to suppress the huge background events and select the most relevant events, we introduce several preselection cuts listed below.

1. Only the events with 4 or 5 jets are considered, including at least 2 tagged b-jets. The transverse momentum of jets are required $P_t(j) > 30$ GeV.

2. The events with exactly 2 isolated photons with $P_t(\gamma) > 30$ GeV are selected.

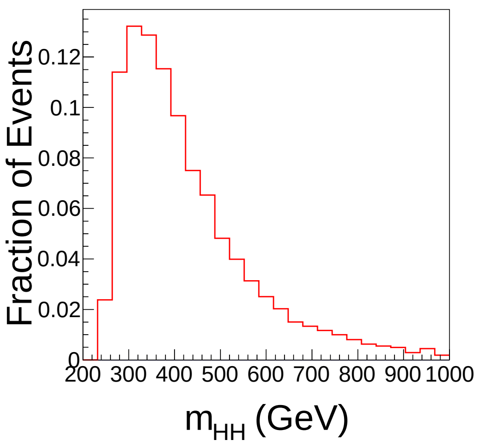

(a)

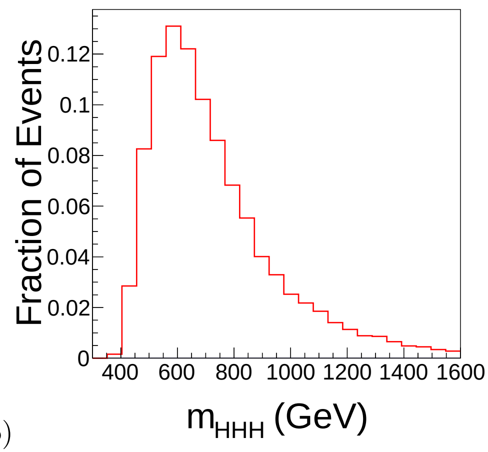

(b)

FIG. 1. Distributions of (a) invariant mass of two Higgs m_{HH} and (b) invariant mass of three Higgs m_{HHH} at the leading order parton level are shown.

3. For $pp \to t\bar{t}H$ background with fully hadronic $t\bar{t}$ decays, where top quark decays to b and W^+, we require that the number of jets reconstructed by the detector should be no more than 5. The distribution of the number of jets for this type of background is shown in Fig. 2(a), which explains why we only consider events with the number of jets 4 and 5.

4. For $pp \to t\bar{t}H$ background with semi-leptonic and dileptonic $t\bar{t}$ decays, where $W^{\pm}$ decays to lepton and neutrino, the detector can reconstruct leptons and a large missing transverse energy (MET). In order to suppress these two types of backgrounds, we veto the events with any leptons. Details about the detector simulation for leptons are shown in Appendix A. As the leptons and all other visible objects are reconstructed, the MET can be reconstructed. The distribution of MET is shown in Fig. 2(b), where one can clearly see that the background has a large MET. However, the MET of $Ht\bar{t}$ events are typically much larger than the signal, so the events with MET > 50 GeV are vetoed.

We would like to have one comment on the first two cuts. These two cuts are quite essential in order to suppress the QCD background from the processes $pp \to 4j2\gamma$. The cross section of the cross section is computed by the package alpgen [44], which yields a result 14.6 pb. After imposing the mass window cut 110GeV $< m_{\gamma\gamma} <$ 140 GeV, the cross section of $pp \to 4j2\gamma$ is around 2.3 pb, which is still around 10 times larger than the main background

$pp \to 2b2j2\gamma$. But after being required at least two tagged b jet, this type of background without charm is suppressed by a factor 10^{-5}, the total cross section of background is less than 2 fb, which is less than 2 percent of the main background $pp \to 2b2j2\gamma$ in our analysis. The background with $2c2j2\gamma$ could have a similar cross section (5.8 pb) as that of $pp \to 2b2j2\gamma$, but after the first two cuts and the mass window cut the contribution of this type of background is only 8 fb or so, which is 4 percent of that of $2b2j2\gamma$ due to the mistagging rate is assumed to be 0.1 in contrast to the tagging efficiency of b jet which is assumed to be 0.6. Therefore, due to these two cuts, we simply omit the background events from the processes $pp \to 4j2\gamma$ and $pp \to 2c2j2\gamma$ in the following analysis.

All the preselection cuts are summarized in TABLE I. After these cuts, the number of events are listed in TABLE II. The results given in Table (II) explicitly demonstrate that the background events are so huge that the observation of triple-Higgs production is very challenging if no more analysis is conducted.

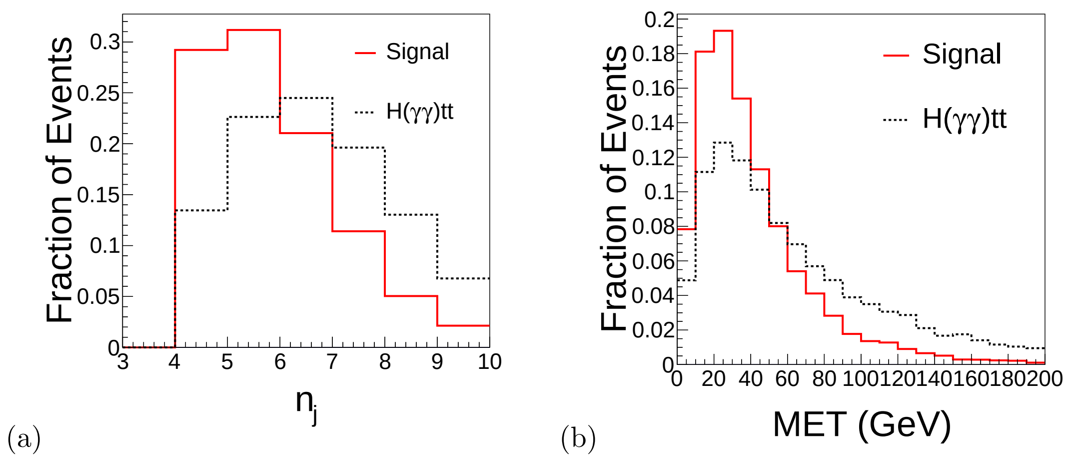

FIG. 2. The distributions of (a) number of jets for the fully hadronic final states and (b) missing energy transverse for the semi-leptonic and dileptonic final states for both signal and the background $pp \to t\bar{t}H$ at the detector level are demonstrated.

To further suppress the background by using the kinematics of the signal, we reconstruct Higgs mass by introducing a χ^2 method, where χ^2 is defined as

$$\chi^2_H(m) = \frac{|M(j_1, j_2) - m|^2}{\sigma_j^2} + \frac{|M(j_3, j_4) - m|^2}{\sigma_j^2} + \frac{|M(\gamma, \gamma) - m|^2}{\sigma_\gamma^2}. \tag{3}$$

Preselection Cuts	Description
1	Number of tagged b-jets $n_b \geq 2$ and $P_t(j) > 30$ GeV with $4 \leq n_j \leq 5$
2	Number of photons $n_\gamma = 2$ with $P_t(\gamma) > 30$ GeV
3	Number of leptons $n_l = 0$
4	Missing energy cut MET$<$ 50 GeV

TABLE I. The preselection cuts in our analysis.

	$\sigma \times BR$ (fb)	K factors	Events after preselection cuts
Signal	9.5×10^{-3}	2.0	50
$b\bar{b}jj\gamma\gamma$	1.9×10^{2}	1.0	2.3×10^{5}
$H(\gamma\gamma)t\bar{t}$	77	1.2	2.2×10^{4}
S/B	1.9×10^{-4}		
$S/\sqrt{S+B}$	9.8×10^{-2}		

TABLE II. The total cross section and the number of events after preselection. Here total integrated luminosity is 30 ab^{-1}. To appreciate the efficiency of each cut, the values of S/B and $S/\sqrt{S+B}$ are provided. For the signal and $H(\gamma\gamma)t\bar{t}$ background, we adopt a K-factor of 2.0 [30] and 1.2 [45] respectively. The K-factor for $b\bar{b}jj\gamma\gamma$ background is not shown in literature. We take a representative value of 1.0. Discussions on its estimated value and its impacts on our results are presented in the Section VI.

Here $M(j_1, j_2)$ and $M(j_3, j_4)$ are the invariant mass of arbitrary two hard jets pair of the events, and $\sigma_j = 10$ GeV is the uncertainty of resolving two jets. $M(\gamma, \gamma)$ is the invariant mass of photons, and $\sigma_\gamma = \sqrt{2}$ GeV is the uncertainty of resolving a pair of photons. All combinations of pairing jets are considered and the reconstruction mass m_H^{rec} is chosen as the m which minimizes χ^2_H. The distribution of the minimum of χ^2_H is shown in Fig. 3(a). Here we have combined $b\bar{b}jj\gamma\gamma$ events and $Ht\bar{t}$ events based on their weights in the total background. It can be seen that the background tends to have a large $\chi^2_{H,min}$, so we can introduce a cut $\chi^2_{H,min} < 6.1$ to suppress the background.

Because the Higgs boson in a $Ht\bar{t}$ event decays to two photons, we noticed that the cut on $m_{\gamma\gamma}$ or m_H^{rec} cannot suppress this type of background effectively. In order to veto such type of background, we reconstruct the top by three jets. We use the reconstruction method

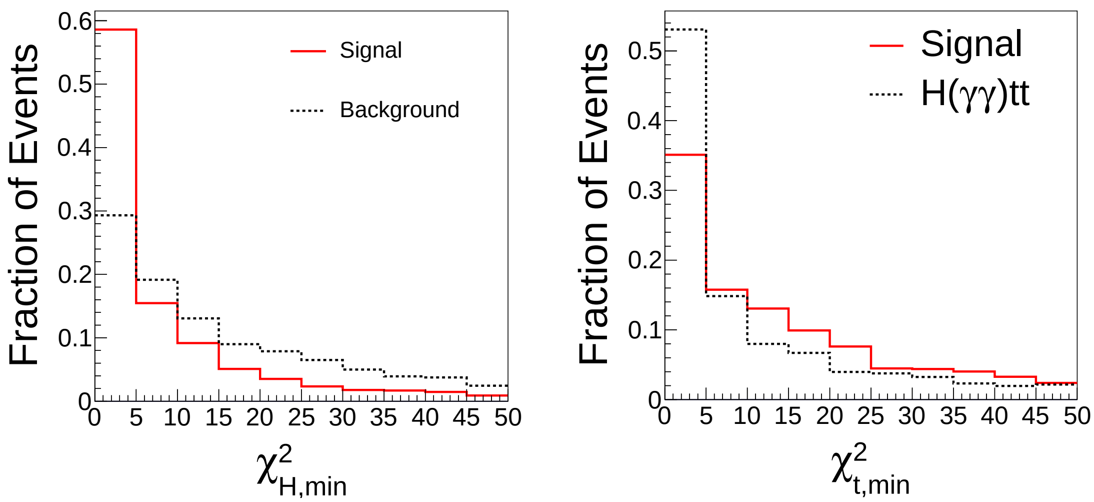

(a)χ^2_H in the Higgs reconstruction

(b)χ^2_t in the Higgs reconstruction

FIG. 3. The distribution of the minimum of χ^2 are shown.

described in [46], where a χ^2 for top reconstruction is

$$\chi^2_t = \frac{|M(j_1, j_2, j_3) - m_t|^2}{\sigma_t^2} + \frac{|M(j_1, j_2) - m_W|^2}{\sigma_W^2}. \tag{4}$$

Here $m_t = 173$ GeV is the top mass, $m_W = 80.4$ GeV is the W mass, $\sigma_t = 15$ GeV and $\sigma_W = 10$ GeV. The reconstructed top mass and W mass are defined as $M^t_{rec} = M(j_1, j_2, j_3)$ and $M^W_{rec} = M(j_1, j_2)$ when χ^2_t is minimum. In the top reconstruction, all combinations of paring jets are considered and we require that $M(j_1, j_2)$ does not include b-jets if only two jets are tagged. The distribution of the minimum of χ^2_t is shown in FIG. 3(b).

The reconstructed top and W masses are shown in FIG. 4. There are peaks around $m_t^{rec} = 173$ GeV and $m_W^{rec} = 80$ GeV both in the signal and backgrounds due to the constraint in the definition of χ^2_t. However, there is another peak around $m_W^{rec} = 126$ GeV in FIG. 4(b), which indicates that these jets have decayed from the Higgs boson.

We are interested in three invariant mass variables: the reconstructed Higgs mass (m_H^{rec}), the invariant mass of the hadronic Higgs bosons (m_{HH}), and the total invariant mass of Higgs bosons (m_{HHH}). They can be extracted after the reconstruction of Higgs bosons. The distribution of these observables are shown in Fig. 5. In FIG. 5(a), there is a peak around $m_H^{rec} = 126$ GeV of signal, but the distribution of background is flat at the region 100 GeV$< M_H <$ 150 GeV, which is consistent with the cuts we imposed at the generator level. After taking the resolution power of photons into consideration, we introduce a reconstructed

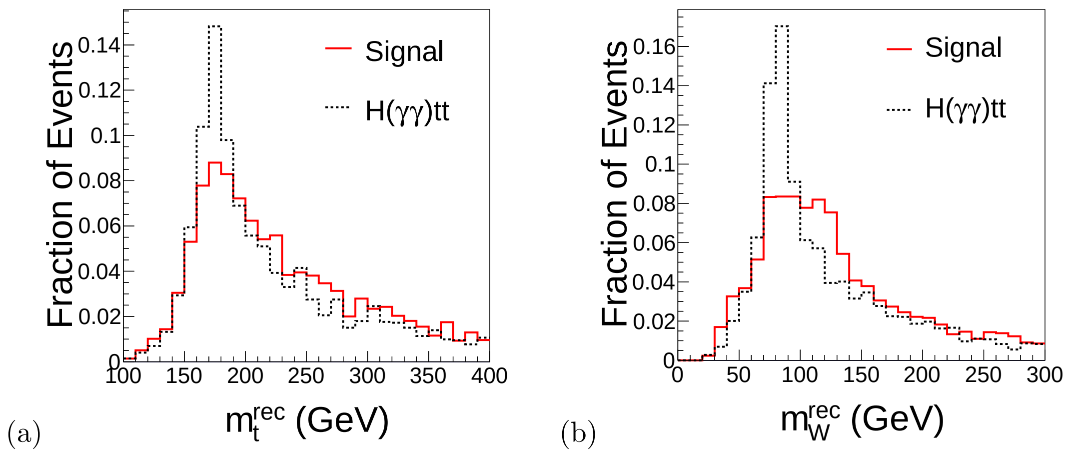

FIG. 4. The distributions of (a) reconstructed top mass and (b) reconstructed W mass.

mass cut $|m_H^{rec} - 126 \text{ GeV}| < 5$ GeV. FIG. 5(b) shows the distribution of the invariant mass of photons. The decay width effect of Higgs boson is not considered in our analysis, so the broadening of the peak in invariant mass $m_{\gamma\gamma}$ is attributed to the detector effects. The invariant mass of photons gives a strong constraint on m_H^{rec}, so a peak can be observed in FIG. 5(a). The peak of Higgs boson mass is reconstructed from a di-photon rather than photons from QCD, as shown in FIG. 5(a) and FIG. 5(b). The invariant mass of two Higgs bosons which decay to $b\bar{b}b\bar{b}$ and total invariant mass of triple-Higgs, respectively are shown in FIG. 5(c) and FIG. 5(d). Because of the detector effects, the distributions of these observables are broadened when compared with those at parton-level ones given in Fig. (1(a)) and Fig.(1(b)).

All cuts we introduced are concluded in TABLE III. This result shows that the cuts we have introduced can enhance S/B by almost one order of magnitude, but cannot improve $S/\sqrt{S+B}$ too much. The smallness of the signal cross section and the detector effects prevent effective background suppression.

C. Multivariate analysis

We apply two multivariate analysis approaches, 1) Boost Decision Tree (BDT) and 2) Multi Layer Perceptron (MLP) neural network, to utilize the correlation of observables in the signal to further suppress backgrounds. In this case, we only consider the events with

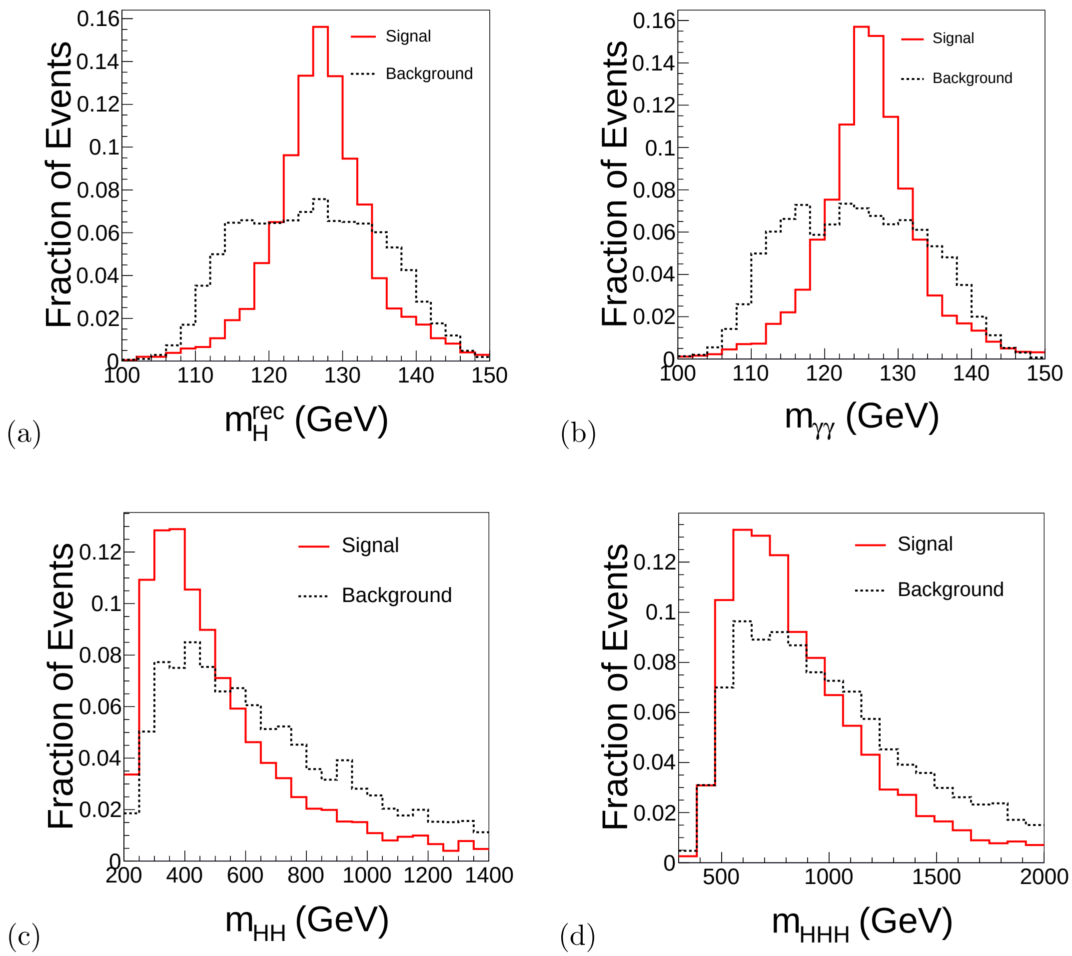

FIG. 5. The distributions of (a) recontructed Higgs mass, (b) invariant mass of two photons, (c) invariant mass of the hardronic Higgs, and (d) the total invariant mass of three Higgs.

	Signal	$b\bar{b}jj\gamma\gamma$	$Ht\bar{t}$
preselection	50	2.3×10^5	2.2×10^4
$\chi^2_{H,min} < 6.1$	26	4.6×10^4	9.9×10^3
$\lvert m_H^{rec} - 126 \text{ GeV}\rvert < 5.1$ GeV	20	1.7×10^4	7.0×10^3
S/B	8.3×10^{-4}		
$S/\sqrt{S+B}$	0.13		

TABLE III. The efficiency of the cuts are demonstrated. Here total integrated luminosity is 30 ab^{-1}. To appreciate the efficiency of each cut, the values of S/B and $S/\sqrt{S+B}$ are provided.

4 jets exactly, and do not introduce any cuts on MET. The observables $P_t(j_i)$, $P_t(\gamma_i)$, $\eta(j_i)$ and $\eta(\gamma_i)$ are considered, where $i = 1, 2, 3, 4$ for jets and $i = 1, 2$ for photons. In addition, the observables we discussed above (MET, $\chi_{H,min}$, $\chi^2_{t,min}$, m_H^{rec}, $m_{\gamma\gamma}$, m_{HH}, m_{HHH}, m_t^{rec} and m_W^{rec}) are also used.

The results are presented in FIG. 6, and the efficiencies are summarized in TABLE IV. The BDT method can increase the value $S/\sqrt{S+B}$ to 0.20, which can be much better than that of the simple cut method. But it is still far from the discovery of triple-Higgs signal.

To observe the triple-Higgs signal of the SM at 5σ level, a much larger integrated luminosity is necessary. TABLE V shows the values of $S/\sqrt{S+B}$ at different integrated luminosity. There we scale up the integrated luminosity for both signal and background. From the table, we see that the integrated luminosity should be around 1.8×10^4 ab^{-1} if we want to discover the triple-Higgs production via $b\bar{b}b\bar{b}\gamma\gamma$ mode at a 100 TeV machine. If we want to extract the information of λ_4, we need an even larger luminosity, as we can see from Eq. (6), where the coefficient B' of λ_4 is only one eighth of C'. This is indeed challenging when considering the realistic integrated luminosity for the future collider projects, as addressed in Ref. [47].

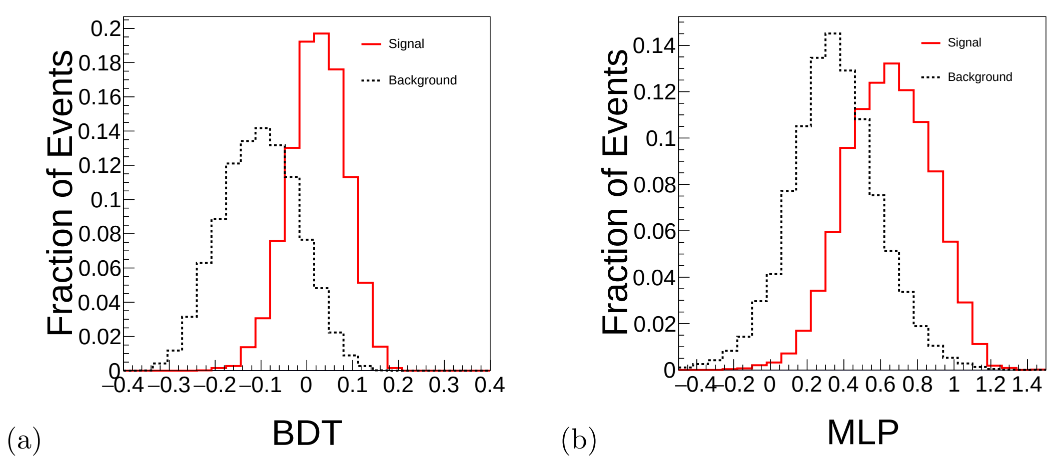

FIG. 6. The response of the discriminants to signal and background in two multivariate analysises, (a) BDT method and (b) MLP neural network method.

IV. THE SENSITIVITY TO QUARTIC COUPLING

It is well known that the process $gg \to HHH$ includes four kinds of Feynman diagrams, as shown in FIG. 7. They are: three Higgs bosons are produced by a pentagon quark-loop

	Cuts based method	BDT> 0.02	MLP> 0.51
Signal	20	34	49
Background	2.4×10^4	2.8×10^4	9.9×10^4
S/B	8.3×10^{-4}	1.2×10^{-3}	5.0×10^{-4}
$S/\sqrt{S+B}$	0.13	0.20	0.16

TABLE IV. The number of events and the significances of the BDT and MLP neural network method are demonstrated. Here total integrated luminosity is 30 ab^{-1}.

Integrated Luminosity (ab^{-1})	30	300	3000	1.83×10^4
$S/\sqrt{S+B}$	0.2	0.6	2.0	5.0

TABLE V. The values of $S/\sqrt{S+B}$ with BDT> 0.02 at different assumed integrated luminosity are displayed.

(FIG. 7(a)), two Higgs bosons are produced by a box quark-loop with a subsequent decay via trilinear coupling (FIG. 7(b)), a Higgs boson is produced by a triangle quark-loop and then decay to three Higgs through two trilinear vertices (FIG. 7(c)), and the triangle quark-loop produce a Higgs boson which decay to three Higgs bosons through quartic coupling (FIG. 7(d)). Only the last kind of diagram involves the quartic coupling.

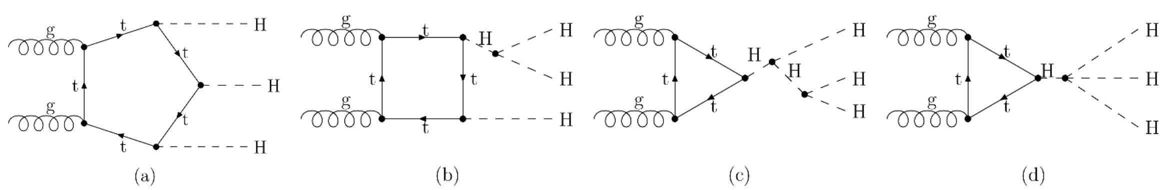

FIG. 7. The example Feynman diagrams of the process $gg \to HHH$ in SM.

To explore the dependence of the cross section of the process $gg \to HHH$ upon the parameters λ_3 and λ_4, we can use the Feynman diagrams as a guide and can parameterize the cross section in the following form

$$\begin{aligned}\sigma(\lambda_3, \lambda_4) &= A\lambda_4^2 + \left(B\lambda_3^2 + C\lambda_3 + D\right)\lambda_4 \\ &\quad + E\lambda_3^4 + F\lambda_3^3 + G\lambda_3^2 + H\lambda_3 + I\,, \end{aligned} \tag{5}$$

where the coefficients A-I can be determined by choosing a certain number of cross section values which are able of to be determined by a set of input pairs of (λ_3, λ_4). It should be pointed out that in this formula we have not included the NLO corrections. We have chosen 21 cross section values in total by using our codes and determined the fitted coefficients A-I, which are tabulated below,

A	B	C	D	E	F	G	H	I
5.28×10^{-2}	0.14	−0.76	0.15	2.28×10^{-2}	-5.36×10^{-2}	3.11	−14.57	15.36

TABLE VI. The fitting coefficients of Eq. 5.

From the fitted coefficients given in Table (VI), there are a few comments in order.

1. The largest three are G, H, and I. I is the contribution of pentagon diagram. The term proportional to G is the contribution of box diagrams. And the term proportional to H corresponds to the interference between the pentagon diagram and box diagrams.

2. The sign of H is opposite to those of G and I. Consequently the total cross section could be sensitive to the sign of λ_3: when λ_3 is positive, it corresponds to a destructive interference; when λ_3 is negative, it corresponds to a constructive interference. It is the former case for the SM.

3. The coefficients A, E and F, are of order (10^{-2}) and are proportional to λ_4^2, λ_3^4, and λ_3^3, respectively. These three terms can only be large when λ_4 and λ_3 are significant.

4. The interference between the triangle and pentagon/box/triangle diagrams are proportional to B, C, and D. It is of the order $\mathcal{O}(10^{-1})$. It should be noticed that the sign of C is different from those of B and D, which indicates that a destructive interference occurs in the SM.

5. When λ_3 is fixed to the SM value , i.e. $\lambda_3 = 1$, the cross section can be simply parameterized as

$$\sigma(\lambda_4) = A\lambda_4^2 + B'\lambda_4 + C' \,. \tag{6}$$

   We find that $B' = -0.47$ and $C' = 3.82$, which are consistent with the formula given in Eq. (5). The fitted cross section and the input cross sections which are red spots as shown in Fig. (8(a)). It shows a good agreement in our numerical results. The minimal value of the cross section happens when $\lambda_4 = 4.46$ and the corresponding cross section is 2.77 fb.

By using the fitted cross section given in Eq. (5) and combining it with our feasibility analysis given in the section above, we explored the projected sensitivity of a 100 TeV collider project to both λ_3 and λ_4 from the measurement of $pp \to hhh$ via $4b$ and 2γ final states. The result is demonstrated in Fig. (8(b)).

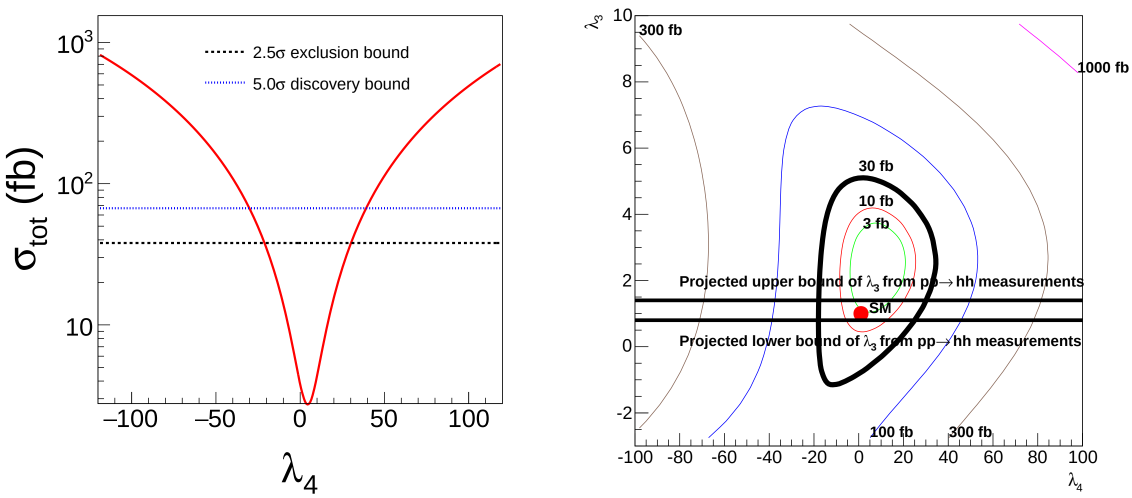

(a) (b)

FIG. 8. (a) The fitted cross section when $\lambda_3 = 1$; (b) The feasibility contours of $\sigma(pp \to hhh)$ in the $\lambda_4 - \lambda_3$ plane.

In Fig. (8(b)), we show 6 contours of cross section which correspond to 1000 fb (pink), 300 fb (yellow), 100 fb (blue), 30 fb (black), 10 fb (red), and 3 fb (green), respectively. It should be noticed that the K-factors of the signal are not included in this plot. If they are included, the results could be better.

Among them, we estimate that the contour with 30 fb is the minimal required cross section for the discovery, which is depicted by a dark line; the contour with 3 fb is depicted by a green line, which is close to the cross section of the SM. In the plot, the big red spot denote the value of the SM. It is worthy of mentioning that to reach 30 fb the value of λ_4 is so large that the perturbativity and the perturbative unitarity are violated.

From the contour with 30 fb, we can read that to discover $gg \to HHH$, the parameter

λ_3 should be confined to the range $[-1, 5]$ and λ_4 should be confined to the range $[-20, 30]$.

For the purpose of comparison, we also depict the projected upper and lower bounds of λ_3 from the measurements of di-Higgs production from the final states $b\bar{b}\gamma\gamma$ [13] and $3\ell 2j + \not{E}$ [21], which could narrow the value of λ_3 down to $1^{+0.4}_{-0.2}$ due to its larger production rate. Accordingly, the parameter λ_4 can be determined into two windows: one is a very narrow one near -20, the other is within $[25, 30]$. In order to distinguish these two windows, further analysis on the shape of distribution is needed. For example, we can separate these two cases by fitting the distribution of transverse momenta of the Higgs boson reconstructed from two photons, an approach which is conducted in [21] by using the tri-lepton invariant mass.

V. TRIPLE-HIGGS PRODUCTION IN THE HIGGS SINGLET MODEL

Although the Higgs boson has been discovered, the direct measurement of Higgs self-couplings are still under confirmation. Exploring the shape of the EW Higgs potential is extremely important and could serve as a window to new physics. Probing Higgs self-couplings can either confirm the SM or discover new physics, which is a No-Lose theorem.

In addition, the matter and antimatter asymmetry has been one of the most fundamental questions in particle physics. A very promising solution is baryogenesis, which requires three criteria to explain the generation of baryon asymmetry observed in the present universe: 1) baryon number violation, 2) C and CP violations, and 3) departure from thermal equilibrium. In the SM the CP violation phase is not big enough. Furthermore, even if the CP violation phase is sufficiently large, for a Higgs with mass at 125–126 GeV, the first order phase transition is not strong enough. This gives us a strong motivation to introduce new physics.

We have learned that the production rate of triple-Higgs events is small in the SM, but it can be enhanced dramatically in a new physics model. One simple extension is adding a real scalar singlet to the SM Higgs sector [48–52]. Moreover, in this model, it is straightforward to produce a strong first order phase transition [6, 7]. In particular, we find that there exists a part of parameter space where the quartic couplings play important roles. Although the main discovery channels are still through $H_2 \to WW, ZZ$, and $t\bar{t}$ (which can either be used to determine the value of the mixing angle or put a constraint on it), triple Higgs production can provide another opportunity to directly observe a new heavy scalar if $BR(H_2 \to HHH)$ is sizeable and thus open up the possibility of a precision measurement of the quartic couplings. Therefore we propose a new channel in which a heavy singlet scalar is produced at resonance and decays into three 126 GeV Higgs bosons. We point out that in this part of parameter space, the resonant di-Higgs production is highly suppressed and the resonant triple Higgs production becomes an important channel to look for the new heavy singlet scalar.

In the singlet+SM model, the Higgs potential can be parameterized as [52]

$$
\begin{aligned}
V(\phi_0, S) = {}& \lambda \left(\phi_0^2 - \frac{v_{EW}^2}{2}\right)^2 + \frac{a_1}{2}\left(\phi_0^2 - \frac{v_{EW}^2}{2}\right) S + \frac{a_2}{2}\left(\phi_0^2 + \frac{v_{EW}^2}{2}\right) S^2 \\
& + \frac{1}{4}\left(2b_2 + a_2 v_{EW}^2\right) S^2 + \frac{b_3}{3} S^3 + \frac{b_4}{4} S^4,
\end{aligned}
\tag{7}
$$

where ϕ_0 is the neutral component of Higgs doublet and S is the additional real singlet. ϕ_0 is expressed as $\phi_0 = (h + v)/\sqrt{2}$, where v is the vev of the doublet. Similarly, the vev of singlet is denoted as x. In the limit of $(v, x) = (v_{EW}, 0)$, the EWSB is minimized.

After EWSB, a new Higgs boson, H_2, is introduced by diagonalizing the Higgs mass matrix from the gauge eigenstates into the mass eigenstates. The mixing angle θ and the parameters of Eq. (7) satisfy following relations:

$$
a_1 = \frac{m_H^2 - m_{H_2}^2}{v_{EW}} \sin 2\theta, \tag{8}
$$

$$
b_2 + \frac{a_2}{2} v_{EW}^2 = m_H^2 \sin^2\theta + m_{H_2}^2 \cos^2\theta, \tag{9}
$$

$$
\lambda = \frac{m_H^2 \cos^2\theta + m_{H_2}^2 \sin^2\theta}{2 v_{EW}^2}. \tag{10}
$$

Above $m_H = 126$ GeV and m_{H_2} is the mass of H_2. Given $(v, x) = (246\ \text{GeV}, 0)$, the remaining free parameters of SM+S are

$$
m_{H_2},\ \theta,\ a_2,\ b_3,\ b_4.
$$

After EWSB, the Higgs self-interaction (in the mass eigenstates) of SM+S are given by

$$
\begin{aligned}
V_{\text{self}} \supset {}& \frac{\lambda_{111}}{6} H^3 + \frac{\lambda_{211}}{2} H^2 H_2 + \frac{\lambda_{221}}{2} H H_2^2 + \frac{\lambda_{222}}{6} H_2^3 \\
& + \frac{\lambda_{1111}}{24} H^4 + \frac{\lambda_{2111}}{6} H^3 H_2 + \frac{\lambda_{2211}}{4} H^2 H_2^2 + \frac{\lambda_{2221}}{6} H H_2^3 + \frac{\lambda_{2222}}{24} H_2^4.
\end{aligned}
\tag{11}
$$

Expressions for above cubic and quartic couplings in terms of m_{H_2}, θ, a_2, b_3, b_4 are listed in [52].

The introduction of the heavy Higgs, H_2, adds five kinds of diagrams to the process $gg \to HHH$. They are: box quark loop $\to H(H_2) \to H(HH)$ (FIG. 9(a)); triangle quark-loop

$\to H_2 \to H(H_2^*) \to H(HH)$ (FIG. 9(b)); triangle quark-loop $\to H_2 \to H(H^*) \to H(HH)$ (FIG. 9(c)); triangle quark-loop$\to$ $H \to H(H_2^*) \to H(HH)$ (FIG. 9(d)); and the triangle quark-loop$\to$ $H_2 \to HHH$ (FIG. 9(e)). The first four diagrams all involve the trillinear coupling λ_{211}. The last diagram instead contain the quartic coupling λ_{2111}.

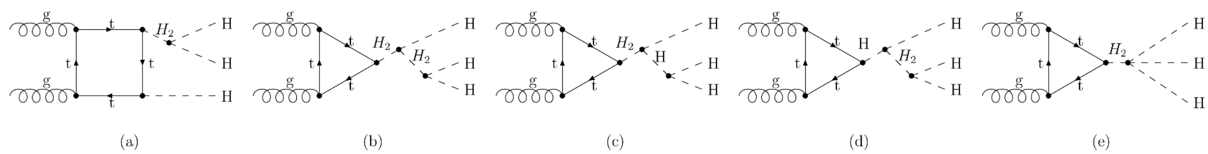

FIG. 9. Extra Feynman diagrams which contribute to the process $gg \to HHH$ in the Higgs singlet model are provided.

We chose benchmark points that introduce a resonance of $H_2 \to HHH$ where the triple-Higgs production is enhanced and other decay channels of H_2 are suppressed. Besides we require the benchmark points satisfy the Higgs vacuum stability requirement, i.e., the Higgs potential at extrema $(v, x) = (v_{EW}, 0)$ is no larger than those at other eight potential local extrema[3].

In the parameter scan, we require

$$378 \text{ GeV} \leq m_{H_2} \lesssim 2 \text{ TeV}, \tag{12}$$

where the lower limit is set by requiring on-shell triple Higgs final states and the upper limit is from the perturbative unitarity constraint. We adopt the restriction $\sin\theta^2 \leq 0.12$ on θ from fittings of the Higgs coupling strengths [53]. We also constrain

$$|a_2| \leq 4\pi, \quad |b_3|/v_{EW} \leq 4\pi, \quad 0 < b_4 \lesssim 8\pi/3, \quad 0 < \lambda \leq 4\pi/3, \quad a_2^2 < 4\lambda b_4. \tag{13}$$

from requirements of perturbative unitarity, perturbativity and the positivity of the potential. The perturbative unitarity bounds above are obtained as following: we compute the normalized spherical amplitude matrix for quadratic scattering between $W_L^+ W_L^-$, $Z_L Z_L$, HH, HH_2 and $H_2 H_2$. Then we require the real parts of the eigenvalues of the matrix to be smaller than $1/2$ [48, 54–56]. Under a good approximation, we take the limit $\theta \to 0$. This

[3] The nine potential local extrema of the Higgs potential are $(v, x) = (v_{EW}, 0)$, $(-v_{EW}, 0)$, (v_+, x_+), $(-v_+, x_+)$, (v_-, x_-), $(-v_-, x_-)$, $(0, x_1^0)$, $(0, x_2^0)$ and $(0, x_3^0)$. Detailed expressions are given by Eq. 24 and Eq. B1 in [52])

	B1	B2	B3
m_{H_2} (GeV)	460	500	490
θ	0.354	0.354	0.354
a_2	3.29	3.48	3.43
b_3 (GeV)	-706	-612	-637
b_4	8.38	8.38	8.38

TABLE VII. The benchmark points to probe the singlet+SM model.

	B1	B2	B3
$\Gamma_{\rm tot}(H_2)$ (GeV)	5.6	7.5	7.0
$BR(H_2 \to W^+W^-)$	0.57	0.56	0.57
$BR(H_2 \to ZZ)$	0.27	0.27	0.27
$BR(H_2 \to t\bar{t})$	0.15	0.16	0.16
$BR(H_2 \to b\bar{b})$	3.4×10^{-4}	2.8×10^{-4}	2.9×10^{-4}
$BR(H_2 \to HH)$	5.3×10^{-7}	8.8×10^{-7}	1.5×10^{-7}
$BR(H_2 \to HHH)$	1.0×10^{-3}	1.4×10^{-3}	1.3×10^{-3}
$\sigma(gg \to H_2)$ @ 14 TeV (fb)	3.2×10^2	2.3×10^2	2.5×10^2
$\sigma(gg \to HHH)$ @ 14 TeV (fb)	0.70	0.69	0.71
$\sigma(gg \to H_2)$ @ 100 TeV (fb)	1.4×10^4	1.1×10^4	1.2×10^4
$\sigma(gg \to HHH)$ @ 100 TeV (fb)	37	38	39

TABLE VIII. The total width and branching ratios of H_2. The cross sections of $gg \to H_2$ and $gg \to HHH$ are listed to demonstrate the enhancement due to the resonance.

leads to restrictions $\lambda \lesssim 4\pi/3$ and $b_4 \lesssim 8\pi/3$. The former restriction yields an upper limit on m_{H_2} as shown in Eq. 12.

The benchmark points are listed in VII. They are obtained by optimizing the cross section for $pp \to H_2 \to HHH$ under the narrow width approximation ($\sigma(pp \to H_2 \to HHH) \approx \sigma(gg \to H_2) \times BR(H_2 \to HHH)$, here we only consider H_2 production via gluon fusion). We found a maximal triple Higgs production cross section is in coincidence with a minimal $BR(H_2 \to HH)$.

There are a few comments in order on these benchmark points:

1. It is remarkable that the resonance of H_2 can enhance the production of triple Higgs boson final state by one order of magnitude for the benchmark points.

2. Enhancements in other channels, like ZZ, could be marginally feasible at the LHC Run 2. Meanwhile, the triple Higgs boson final states could also be reachable for the LHC high luminosity run (HL-LHC). For a 100 TeV collider, both ZZ and triple Higgs boson final states could be reachable.

3. Enhancements in di-Higgs boson final states can be safely neglected due to the tiny branching fraction of $H_2 \to HH$.

We implement the model based on the loop_sm module in MadGraph5/aMC@NLO [40]. Firstly, we add the model parameters, then implement all the relevant vertices and couplings. As well as the tree level vertices, the relevant vertices for R2 terms are also added according to Ref. [57].

The triple-Higgs events at this model can be generated efficiently by the new version of MadGraph5/aMC@NLO [58], which can handle the loop-induced process. To perform the feasibility study, we generate 40,000 events for each benchmark point. We conduct the same analysis as demonstrated in the previous sections. Here we present our results on these three benchmark points in FIG. (10) and TABLE IX.

FIG. 10(a) shows the invariant mass of triple Higgs boson on three benchmark points. Comparing to the SM signal and background, the distributions of B1 and B2 has a resonance peak around 450 GeV and 500 GeV, respectively. These peaks are close to the peak from pentegon diagrams, so the resonance peaks are broadened. FIG. 10(b) shows the invariant mass of di-Higgs bosons. When the new diagrams are introduced, the invariant mass of three Higgs bosons tends to be around threshold around 300 GeV. Because the branching ratio $BR(H_2 \to HH) \approx 0$ in B1 and B2, there are not peak around the mass of m_{H_2}.

TABLE IX shows the significances of these three benchmark points. It is observed that the significances can be improved from 0.2 to 2.1, 2.5 and 2.3, respectively. To obtain these numbers, we estimate the production rate by multiplying the LO cross section computed by the MG5 with a K-factor extracted from the reference [59] where N^{3}LO QCD corrections and NLO EW corrections for $gg \to H_2$ have been taken into account. There are two reasons

	SM(BDT>0.02)	B1(BDT>-0.02)	B2(BDT>-0.02)	B3(BDT>-0.03)
Signal	34	3.7×10^2	4.4×10^2	4.6×10^2
Background	2.8×10^4	3.0×10^4	3.1×10^4	4.0×10^4
S/B	1.2×10^{-3}	1.2×10^{-2}	1.4×10^{-2}	1.1×10^{-2}
$S/\sqrt{S+B}$	0.20	2.1	2.5	2.3

TABLE IX. The numbers of events and the efficiencies of the BDT method on SM and the three benchmark points of the singlet+SM model. Here total integrated luminosity is 30 ab^{-1}.

to do so: 1) H_2 couples to top quark is similar to that of the SM-like Higgs boson. Its coupling strength is equal to $y_t \sin(\theta)/\sqrt{2}$; 2) the contribution of $gg \to H_2 \to HHH$ is the overwhelming process for the triple Higgs boson production in these benchmark points. As described above, the new resonance can enhance one order of magnitude of the triple-Higgs production rate. Moreover, the new cuts from the invariant mass of triple Higgs and di-Higgs can also improve the discrimination of signal and background events. Therefore, we use the K-factor of $gg \to H_2$ to estimate the K-factor of $gg \to H_2 \to HHH$. It is noticed that this agrees with the K-factor computed in the reference [60].

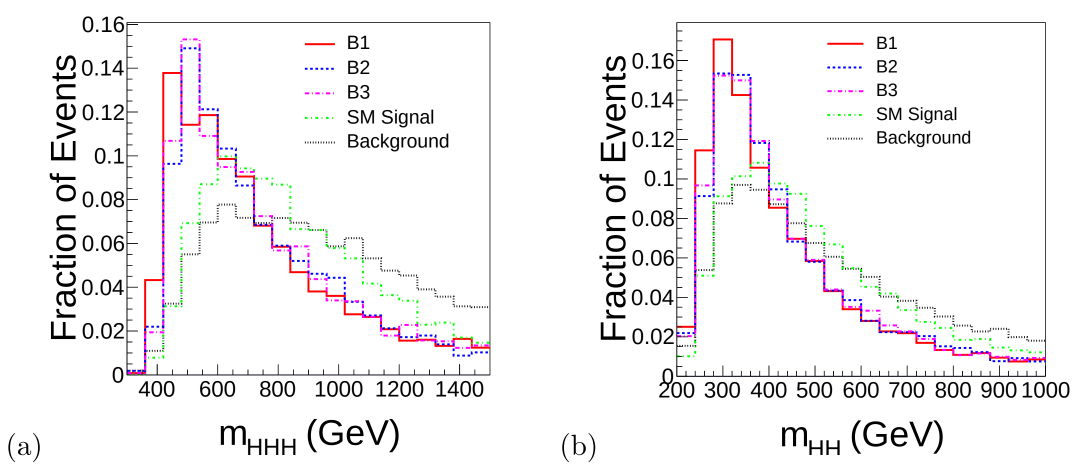

FIG. 10. The detector level distributions of (a) invariant mass of three Higgs bosons and (b) invariant mass of di-Higgs bosons on three benchmark points of the singlet+SM model, comparing with the distributions of SM signal and backgrounds.

VI. DISCUSSION AND CONCLUSION

In this paper, we have studied the feasibility of triple Higgs production via $4b2\gamma$ final states at a 100 TeV hadron collider. We explore some kinematic cuts which can reduce background effectively. And we find it is challenging to measure the quartic coupling of the Higgs boson in the SM even at a 100 TeV hadron collider if luminosity is assumed to be 30 ab^{-1} due to its small cross section and the huge QCD background. In order to observe the signal of the SM, an integrated luminosity up to 1.8×10^4 ab^{-1} is required.

If new physics is taken into account that can enhance the triple Higgs production rate, it is promising to discover triple-Higgs production via $b\bar{b}b\bar{b}\gamma\gamma$ channel. For the effective Higgs potential model introduced in Eq. (1), we find that λ_3 can be confined to the range $[-1, 5]$ and λ_4 can be confined to the range $[-20, 30]$.

In our detector simulation, we have assumed that b-tagging efficiency at most is around 60%. According to the current results from both CMS and ATLAS collaborations, the b-tagging efficiency can reach up to around 70%. Therefore we can expect that a better result could be yielded when a larger b-tagging efficiency is taken.

In above analysis, we have applied a b-tagging cut at $n_b \geq 2$. We also expose other n_b cases in Table B. It is found that the analysis with either $n_b \geq 2$ or $n_b \geq 3$ is the best. For $n_b \geq 3$, the signal events are lost by a factor of 60%, but the background events $pp \to b\bar{b}jj\gamma\gamma$ and $pp \to H(\gamma\gamma)t\bar{t}$ are suppressed by one order of magnitude. Although the background $pp \to b\bar{b}b\bar{b}\gamma\gamma$ becomes as important as $pp \to H(\gamma\gamma)t\bar{t}$, we obtain a better S/B and $S/\sqrt{S+B}$.

Although most of the signal events are kept for $n_b \geq 1$, backgrounds there are substantial. They are three times larger than those for $n_b \geq 2$. Besides, QCD contributes a huge background of $4j2\gamma$ with one light-jet faking a b-jet. On the other extreme, $n_b \geq 4$ can effectively suppress the background (a factor of $\mathcal{O}(10)$ less than $n_b \geq 3$). But the signal then suffers a huge loss that leads to a low significance. Analysis of the case $n \geq 4$ should only be considered if the production rate of signal is sufficiently large, such as in the singlet+SM model.

It is interesting to explore the underlying reasons for the loss of signal events in both $n_b \geq 3$ and $n_b \geq 4$ analyses. Such a loss can be expected from the b-tagging efficiency characterized by Eq. (B1). One find that the hardest b-tagging jet has a peak around 120

	$n_b \geq 1$	$n_b \geq 2$	$n_b \geq 3$	$n_b \geq 4$
SM signal	79	50	18	2.8
$b\bar{b}jj\gamma\gamma$	7.0×10^5	2.3×10^5	1.8×10^4	850
$H(\gamma\gamma)t\bar{t}$	7.0×10^4	2.2×10^4	1.7×10^3	21
$b\bar{b}b\bar{b}\gamma\gamma$	5.1×10^3	3.6×10^3	1.4×10^3	260
S/B	1.0×10^{-4}	1.9×10^{-4}	8.5×10^{-4}	2.5×10^{-3}
$S/\sqrt{S+B}$	8.9×10^{-2}	9.8×10^{-2}	0.12	8.3×10^{-2}

TABLE X. The significances for analyses with different number of tagged b-jets. Here the luminosity is 30 ab^{-1}.

GeV, while the second hardest jet has a peak around 50 GeV. Based on Eq. (B1), the b-tagging efficiency ϵ_b reduces to 0.4 when $P_t(j) \sim 50$ GeV. In the events with 3 or more b-tagged jets, the third hardest jet has a transverse momentum less than 50 GeV and ϵ_b is further reduced, which leads to a 50% loss of signal events. It becomes even worse when we require $n_b \geq 4$, where the peak of the transverse momentum of the fourth hardest jet is less than 30 GeV and the b-tagging efficiency is dropped down to less than 0.3, as demonstrated in Table (XII). FIG. 11 shows the transverse momentum of the third and fourth hardest tagged b-jets, which provide evidence why the signal events suffer a big loss when we increase the number of tagged b-jets. It will be greatly helpful for the triple Higgs discovery if the detectors of future colliders can improve the b-tagging efficiency for soft b-jets.

We find Ref. [30] has done a similar study on triple-Higgs productions but with only the case $n_b \geq 4$ considered. The authors show that a signal-to-background ratio can reach ~ 1 at a 100 TeV hadron collider, which requires a high b-tagging efficiency (80%), a low light-jet mis-tagging rate (1%) and excellent photon identification. We have focused on the case $n_b \geq 2$ instead. We show that an important background $pp \to bbjj$ could contribute significantly in those cases $n_b \geq 2$, $n_b \geq 3$ and $n_b \geq 4$ Meanwhile, the process $pp \to t\bar{t}H$ can contribute around 30% of the total background of the SM in the case $n_b \geq 2$. After taking into account more realistic b-tagging efficiency, especially those soft b jets in signal events, our analysis shows that the discovery of the signature of triple Higgs final state in the SM is indeed challenging.

In the model where an extra Higgs singlet is added to the SM, we propose a few benchmark

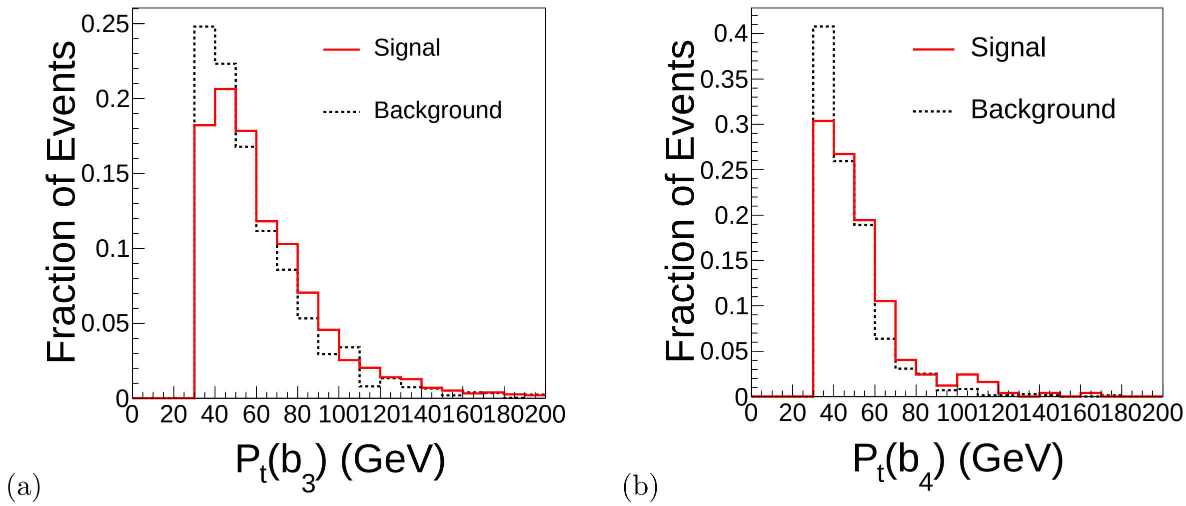

FIG. 11. The transverse momentum distributions of (a) the third and (b) the fourth hardest tagged b-jets.

points where the production rate of $gg \to HHH$ can be enhanced dramatically by new resonances. Due to the existence of resonances, we can have more efficient kinematic cuts to suppress the SM background. In our work, the efficiency can be up to 2.5 on benchmark point B2 when the luminosity is 30 ab^{-1}.

In our analysis, the K-factor of $2b2j2\gamma$ is assumed to be 1. We may also use the result computed for the process $pp \to 4b$ [61] to estimate it, where K-factor is around 1.4. Since this is the main background for the signal channel, our results could be significantly affected by this factor. But our results could serve as a guide to estimate the required luminosity. Meanwhile, this work indicates that the QCD corrections of the process $pp \to 2b2j2\gamma$ could be important for triple Higgs production and should be studied carefully.

Here we would like to address the fake photon issue. The high energy neutral pions can fake photons in the ECAL. The cross section of the processes $pp \to 2b4j$ and $pp \to 2b3j\gamma$ are found by using Alpgen[44] to be 2.1×10^5 pb and 250 pb, respectively. When the fake photon rate is assumed to be 0.1%, the cross sections are dropped down to 1260 fb and 750 fb (combinatorial factors have been taken into account), respectively. After the invariant mass window cut on the diphoton invariant mass, we noticed that only around 10% events can contribute like events $2b2j2\gamma$. Then we noticed that the combination of these type of background can be of the same size as $pp \to 2b2j2\gamma$. This will make the minimum luminosity even larger by the number estimated in Table (V). The minimum luminosity derived from the results of mode $n_b \geq 3$ could be more robust than that of the mode $n_b \geq 2$ after taking into account the contribution of fake photon events to the main background $2b2j2\gamma$ and the minimal luminosity close to that quoted in Table (V). If the fake rate can be further reduced experimentally, then combine both $n_b = 2$ and $n_b = 3$ modes gains us a little in reducing the minimal required luminosity.

The next step of this work is to study the feasibility of other channels, either in the SM or new physics models. The potential discovery channels and their branching ratios for triple-Higgs production are listed in TABLE XI. One can find that the $b\bar{b}b\bar{b}W^+W^-$ channel has the largest branching ratio and the number of signal events should be increased dramatically. However, the SM backgrounds might be too large for this channel. For example, the cross section of $pp \to b\bar{b}t\bar{t}$ can be up to $\sim 10^3$ pb and it could be difficult to reduce such a large background. For the same reason, the $HHH \to b\bar{b}b\bar{b}b\bar{b}$ channel might also be difficult, unless we can find a better way to suppress the background. The channels with more than 4 W bosons might also be feasible. For highly boosted Higgs bosons in the triple Higgs boson final states, the jet substructure techniques, like Higgs-tagger methods [62], could also be investigated. These studies will be carried out in our future projects.

ACKNOWLEDGMENTS

We thank Sally Dawson and Giovanni Marco Pruna for helpful discussions, and Andreas Papaefstathiou for useful communication. The work of Qi-Shu Yan and Xiaoran Zhao are supported by the Natural Science Foundation of China under the grant NO. 11175251 and NO. 11475180. The work of C.-Y. Chen is supported in part by the U.S. Department of Energy under grant No. DE-AC02-98CH10886 and contract DE-AC02-76SF00515 and by NSERC, Canada. Research at the Perimeter Institute is supported in part by the Government of Canada through NSERC and by the Province of Ontario through MEDT. YZ are supported by the U.S. Department of Energy grant DESC0008061.

Decay Channel	Branching Ratio
$HHH \to b\bar{b}b\bar{b}W^+W^-$	22.34%
$HHH \to b\bar{b}b\bar{b}b\bar{b}$	20.30%
$HHH \to b\bar{b}W^+W^-W^+W^-$	8.20%
$HHH \to b\bar{b}b\bar{b}\tau^+\tau^-$	7.16%
$HHH \to b\bar{b}b\bar{b}gg$	6.54%
$HHH \to b\bar{b}b\bar{b}ZZ$	2.69%
$HHH \to W^+W^-W^+W^-W^+W^-$	1.00%
$HHH \to W^+W^-W^+W^-\tau^+\tau^-$	0.96%
$HHH \to W^+W^-W^+W^-gg$	0.88%
$HHH \to W^+W^-W^+W^-ZZ$	0.36%
$HHH \to b\bar{b}b\bar{b}\gamma\gamma$	0.29%

TABLE XI. Some possible discovery channels for triple-Higgs production are listed. Channels with branching fraction less than 0.1% are omitted.

Appendix A: Set-up for the detector simulation

In the detector simulation, the radius and half-length of the magnetic field coverage are assumed to be 3.0 m and 5.0 m, respectively. The axial magnetic field is 5.0 T. The energy resolution formula of electromagnetic calorimeter (ECAL) is assumed to be

$$\sigma_{ECAL} = \begin{cases} \sqrt{0.007^2 \left(\frac{E}{\mathrm{GeV}}\right)^2 + 0.07^2 \left(\frac{E}{\mathrm{GeV}}\right) + 0.35^2}, & \text{if } |\eta| \leq 3.0\,, \\ \sqrt{0.107^2 \left(\frac{E}{\mathrm{GeV}}\right)^2 + 2.08^2 \left(\frac{E}{\mathrm{GeV}}\right)}. & \text{if } 3.0 < |\eta| \leq 5.0\,, \end{cases} \tag{A1}$$

The energy resolution formula for hadron calorimeter (HCAL) is assumed to be

$$\sigma_{HCAL} = \begin{cases} \sqrt{0.05^2 \left(\frac{E}{\mathrm{GeV}}\right)^2 + 1.5^2 \left(\frac{E}{\mathrm{GeV}}\right)}, & \text{if } |\eta| \leq 3.0\,, \\ \sqrt{0.13^2 \left(\frac{E}{\mathrm{GeV}}\right)^2 + 2.7^2 \left(\frac{E}{\mathrm{GeV}}\right)}, & \text{if } 3.0 < |\eta| \leq 5.0\,, \\ 0, & \text{otherwise.} \end{cases} \tag{A2}$$

here σ_{ECAL} and σ_{HCAL} are the resolutions of ECAL and HCAL, respectively. They are functions of energy, E, and pseudo-rapidity, η, of charged leptons and jets respectively. In these formulae, the coefficients are taken from the default CMS card in DELPHES, but the regions of η for leptons and jets are extended from ± 2.5 to ± 5.0.

Details for the lepton detection are list as following. The electron efficiency is 95% when $P_t(e) > 10$ GeV and $|\eta(e)| \leq 2.5$, but decreases to 85% when $2.5 < |\eta(e)| \leq 5.0$. For muons, the efficiency is 95% when 10 GeV$< P_t(\mu) \leq 1$ TeV and $|\eta(\mu)| \leq 5.0$. When $P_t(\mu) > 1$ TeV, the muon efficiency satisfies $0.95 \exp[0.5 - P_t(\mu) \times 5.0 \times 10^{-4}]$. The photon efficiency is found to be close to the electron efficiency.

Appendix B: *b*-tagging efficiency curves

We adopt b-tagging efficiency curve at the 60% b-jet efficiency working point. It is given by

$$\epsilon_b = \begin{cases} 0.6 \tanh\left[0.03\left(\frac{P_t(j)}{\mathrm{GeV}}\right) - 0.4\right], & \text{for } |\eta(j)| \leq 2.5, \\ 0.5 \tanh\left[0.03\left(\frac{P_t(j)}{\mathrm{GeV}}\right) - 0.4\right], & \text{for } 2.5 < |\eta(j)| \leq 5.0, \\ 0, & \text{otherwise.} \end{cases} \tag{B1}$$

The corresponding mistagging rate of charm quark is

$$\epsilon_{c\to b} = \begin{cases} 0.1 \tanh\left[0.03\left(\frac{P_t(j)}{\mathrm{GeV}}\right) - 0.4\right], & \text{for } |\eta(j)| \leq 5.0, \\ 0, & \text{otherwise.} \end{cases} \tag{B2}$$

And the corresponding mistagging rate of light quarks and gluons is

$$\epsilon_{j\to b} = \begin{cases} 0.001, & \text{for } |\eta(j)| \leq 5.0, \\ 0, & \text{otherwise.} \end{cases} \tag{B3}$$

The light quarks has a small mistagging rate $\epsilon_{j\to b} = 0.001$ for $|\eta(j)| \leq 5.0$.

In Table (XII), we show how b-tagging efficiency vary with reference to the transverse momentum and η of jets. We would like emphasize that when the transverse momentum of a b-jet is soft, the tagging efficiency is low.

P_t (GeV)	$\epsilon_b(\lvert\eta(j)\rvert \leq 2.5)$	$\epsilon_b(2.5 \leq \lvert\eta(j)\rvert \leq 5)$
120	0.60	0.50
100	0.59	0.49
80	0.58	0.48
50	0.48	0.40
30	0.28	0.23

TABLE XII. The b-tagging efficiency varying with P_t is presented.

[1] G. Aad *et al.* [ATLAS Collaboration], Phys. Lett. B **716**, 1 (2012) [arXiv:1207.7214 [hep-ex]].

[2] S. Chatrchyan *et al.* [CMS Collaboration], Phys. Lett. B **716**, 30 (2012) [arXiv:1207.7235 [hep-ex]].

[3] S. Dawson, A. Gritsan, H. Logan, J. Qian, C. Tully, R. Van Kooten, A. Ajaib and A. Anastassov *et al.*, arXiv:1310.8361 [hep-ex].

[4] M. Trodden, Rev. Mod. Phys. **71**, 1463 (1999) [hep-ph/9803479].

[5] H. J. He, J. Ren and W. Yao, arXiv:1506.03302 [hep-ph].

[6] A. Ahriche, Phys. Rev. D **75**, 083522 (2007) [hep-ph/0701192].

[7] S. Profumo, M. J. Ramsey-Musolf and G. Shaughnessy, JHEP **0708**, 010 (2007) [arXiv:0705.2425 [hep-ph]].

[8] T. Plehn, M. Spira and P. M. Zerwas, Nucl. Phys. B **479**, 46 (1996) [Erratum-ibid. B **531**, 655 (1998)] [hep-ph/9603205].

[9] U. Baur, T. Plehn and D. L. Rainwater, Phys. Rev. D **67**, 033003 (2003) [hep-ph/0211224].

[10] J. Baglio, A. Djouadi, R. Grber, M. M. Mhlleitner, J. Quevillon and M. Spira, JHEP **1304**, 151 (2013) [arXiv:1212.5581 [hep-ph]].

[11] Q. Li, Q. S. Yan and X. Zhao, Phys. Rev. D **89**, 033015 (2014) [arXiv:1312.3830 [hep-ph]].

[12] U. Baur, T. Plehn and D. L. Rainwater, Phys. Rev. D **69**, 053004 (2004) [hep-ph/0310056].

[13] W. Yao, arXiv:1308.6302 [hep-ph].

[14] M. J. Dolan, C. Englert and M. Spannowsky, JHEP **1210**, 112 (2012) [arXiv:1206.5001 [hep-ph]].

[15] A. J. Barr, M. J. Dolan, C. Englert and M. Spannowsky, Phys. Lett. B **728**, 308 (2014) [arXiv:1309.6318 [hep-ph]].

[16] A. Papaefstathiou, L. L. Yang and J. Zurita, Phys. Rev. D **87**, 011301 (2013) [arXiv:1209.1489 [hep-ph]].

[17] D. E. Ferreira de Lima, A. Papaefstathiou and M. Spannowsky, JHEP **1408**, 030 (2014) [arXiv:1404.7139 [hep-ph]].

[18] V. Barger, L. L. Everett, C. B. Jackson and G. Shaughnessy, Phys. Lett. B **728**, 433 (2014) [arXiv:1311.2931 [hep-ph]].

[19] A. J. Barr, M. J. Dolan, C. Englert, D. E. F. de Lima and M. Spannowsky, arXiv:1412.7154

[hep-ph].

[20] A. Papaefstathiou, arXiv:1504.04621 [hep-ph].

[21] Q. Li, Z. Li, Q. S. Yan and X. Zhao, arXiv:1503.07611 [hep-ph].

[22] B. Bhattacherjee and A. Choudhury, Phys. Rev. D **91**, 073015 (2015) [arXiv:1407.6866 [hep-ph]].

[23] A. Djouadi, W. Kilian, M. Muhlleitner and P. M. Zerwas, Eur. Phys. J. C **10**, 27 (1999) [hep-ph/9903229].

[24] G. Ferrera, J. Guasch, D. Lopez-Val and J. Sola, Phys. Lett. B **659**, 297 (2008) [arXiv:0707.3162 [hep-ph]].

[25] G. Ferrera, J. Guasch, D. Lopez-Val and J. Sola, PoS RADCOR **2007**, 043 (2007) [arXiv:0801.3907 [hep-ph]].

[26] M. McCullough, Phys. Rev. D **90**, no. 1, 015001 (2014) [Phys. Rev. D **92**, no. 3, 039903 (2015)] [arXiv:1312.3322 [hep-ph]].

[27] T. Plehn and M. Rauch, Phys. Rev. D **72**, 053008 (2005) [hep-ph/0507321].

[28] T. Binoth, S. Karg, N. Kauer and R. Ruckl, Phys. Rev. D **74**, 113008 (2006) [hep-ph/0608057].

[29] F. Maltoni, E. Vryonidou and M. Zaro, JHEP **1411**, 079 (2014) [arXiv:1408.6542 [hep-ph]].

[30] A. Papaefstathiou and K. Sakurai, arXiv:1508.06524 [hep-ph].

[31] S. Ovyn, X. Rouby and V. Lemaitre, arXiv:0903.2225 [hep-ph].

[32] J. de Favereau *et al.* [DELPHES 3 Collaboration], JHEP **1402**, 057 (2014) [arXiv:1307.6346 [hep-ex]].

[33] R. Pittau, arXiv:1202.5781 [hep-ph].

[34] G. Cullen, H. van Deurzen, N. Greiner, G. Heinrich, G. Luisoni, P. Mastrolia, E. Mirabella and G. Ossola *et al.*, Eur. Phys. J. C **74**, no. 8, 3001 (2014) [arXiv:1404.7096 [hep-ph]].

[35] K. Arnold, M. Bahr, G. Bozzi, F. Campanario, C. Englert, T. Figy, N. Greiner and C. Hackstein *et al.*, Comput. Phys. Commun. **180**, 1661 (2009) [arXiv:0811.4559 [hep-ph]].

[36] K. Arnold, J. Bellm, G. Bozzi, M. Brieg, F. Campanario, C. Englert, B. Feigl and J. Frank *et al.*, arXiv:1107.4038 [hep-ph].

[37] J. Baglio, J. Bellm, F. Campanario, B. Feigl, J. Frank, T. Figy, M. Kerner and L. D. Ninh *et al.*, arXiv:1404.3940 [hep-ph].

[38] J. Pumplin, D. R. Stump, J. Huston, H. L. Lai, P. M. Nadolsky and W. K. Tung, JHEP **0207**, 012 (2002) [hep-ph/0201195].

[39] T. Sjostrand, S. Mrenna and P. Z. Skands, JHEP **0605**, 026 (2006) [hep-ph/0603175].

[40] J. Alwall, R. Frederix, S. Frixione, V. Hirschi, F. Maltoni, O. Mattelaer, H.-S. Shao and T. Stelzer *et al.*, JHEP **1407**, 079 (2014) [arXiv:1405.0301 [hep-ph]].

[41] T. Sjstrand, S. Ask, J. R. Christiansen, R. Corke, N. Desai, P. Ilten, S. Mrenna and S. Prestel *et al.*, arXiv:1410.3012 [hep-ph].

[42] M. Cacciari, G. P. Salam and G. Soyez, Eur. Phys. J. C **72**, 1896 (2012) [arXiv:1111.6097 [hep-ph]].

[43] M. Cacciari, G. P. Salam and G. Soyez, JHEP **0804**, 063 (2008) [arXiv:0802.1189 [hep-ph]].

[44] M. L. Mangano, M. Moretti, F. Piccinini, R. Pittau, A. D. Polosa, JHEP07, (2003) 001 [hep-ph/0206293].

[45] S. Dawson, C. Jackson, L. H. Orr, L. Reina and D. Wackeroth, Phys. Rev. D **68**, 034022 (2003) [hep-ph/0305087].

[46] S. Yang and Q. S. Yan, JHEP **1202**, 074 (2012) [arXiv:1111.4530 [hep-ph]].

[47] I. Hinchliffe, A. Kotwal, M. L. Mangano, C. Quigg and L. T. Wang, Int. J. Mod. Phys. A **30**, no. 23, 1544002 (2015) [arXiv:1504.06108 [hep-ph]].

[48] G. M. Pruna and T. Robens, Phys. Rev. D **88**, no. 11, 115012 (2013) [arXiv:1303.1150 [hep-ph]].

[49] V. Barger, P. Langacker, M. McCaskey, M. J. Ramsey-Musolf and G. Shaughnessy, Phys. Rev. D **77**, 035005 (2008) [arXiv:0706.4311 [hep-ph]].

[50] D. O'Connell, M. J. Ramsey-Musolf and M. B. Wise, Phys. Rev. D **75**, 037701 (2007) [hep-ph/0611014].

[51] S. Profumo, M. J. Ramsey-Musolf, C. L. Wainwright and P. Winslow, Phys. Rev. D **91**, no. 3, 035018 (2015) [arXiv:1407.5342 [hep-ph]].

[52] C. Y. Chen, S. Dawson and I. M. Lewis, Phys. Rev. D **91**, no. 3, 035015 (2015) [arXiv:1410.5488 [hep-ph]].

[53] ATLAS-CONF-2014-010.

[54] B. W. Lee, C. Quigg and H. B. Thacker, Phys. Rev. D **16**, 1519 (1977).

[55] J. F. Gunion, H. E. Haber, G. L. Kane and S. Dawson, Front. Phys. **80**, 1 (2000).

[56] L. Basso, A. Belyaev, S. Moretti and G. M. Pruna, Phys. Rev. D **81**, 095018 (2010) [arXiv:1002.1939 [hep-ph]].

[57] P. Draggiotis, M. V. Garzelli, C. G. Papadopoulos and R. Pittau, JHEP **0904**, 072 (2009)

[arXiv:0903.0356 [hep-ph]].

[58] V. Hirschi and O. Mattelaer, arXiv:1507.00020 [hep-ph].

[59] S. Dittmaier *et al.* [LHC Higgs Cross Section Working Group Collaboration], arXiv:1101.0593 [hep-ph].

[60] S. Dawson and I. M. Lewis, arXiv:1508.05397 [hep-ph].

[61] M. Worek, PoS RADCOR **2013**, 038 (2013) [arXiv:1311.2396 [hep-ph]].

[62] J. M. Butterworth, A. R. Davison, M. Rubin and G. P. Salam, Phys. Rev. Lett. **100**, 242001 (2008) [arXiv:0802.2470 [hep-ph]].